IMAGE REGISTRATION FOR ABDOMINAL DYNAMIC CONTRAST-ENHANCED MAGNETIC RESONANCE IMAGES

Anthony Lausch, Mehran Ebrahimi, Anne Martel

Department of Medical Biophysics, University of Toronto

ABSTRACT

A simple, computationally inexpensive, algorithm for performing registration of abdominal dynamic contrast-enhanced (DCE) MRI data is presented. It utilizes an intensity correction term in conjunction with a so-called floating reference image scheme to reduce the effects of contrast agent related intensity changes on registration performance. Using an abdominal DCE-MRI dataset with simulated motion, it is shown that the algorithm is capable of correcting for non-rigid motion of various magnitudes. The registration also helped to elucidate trends in the enhancement curve of a small region of interest within a renal tumour of a dataset with un-simulated motion. In all cases, evidence of visual motion was almost entirely eliminated after registration. Since the algorithm does not involve altering image registration optimization processes, it is predicted that it should be easily adapted to other registration frameworks.

Index Terms— image registration, biomedical image processing, magnetic resonance imaging

1. INTRODUCTION

Dynamic contrast - enhanced magnetic resonance imaging (DCE-MRI) usually involves the acquisition of images prior to and after the injection of a contrast agent (e.g. Gd-DTPA). The contrast agent diffuses out from the vasculature and accumulates in the interstitial space, producing signal increases in T1-weighted images. These signal intensity increases can be converted to contrast agent concentrations and subsequently used with pharmacokinetic models in order to acquire information regarding blood volume and vascular permeability [7].

DCE-MRI shows promise as a method to evaluate the efficacy of new anti-cancer drugs which seek to inhibit tumour angiogenesis [7]. A primary requirement for accurate DCE-MRI analysis is that image intensity changes are only due to the flow of the contrast agent through the vasculature. However, there is always some motion present (e.g. breathing) which can cause changes unrelated to the contrast agent. This motion results in the inaccurate conversion of signal intensity changes to contrast agent concentrations. Consequently motion reduces the accuracy of blood volume and vascular permeability estimates and subsequent evaluations of therapeutic response [7].

Image registration has been successfully used to eliminate motion within a variety of different settings but is particularly challenging to develop for contrast-enhanced datasets [4]. Traditional image registration techniques assume that image structures can move but that their pixel intensities remain constant in time. Dynamic contrast-enhanced datasets directly violate this assumption. Furthermore, motion present in images due to the flow of the contrast agent must not be eliminated by the image registration as this data is the focus of subsequent analysis.

Here we describe a method for registering abdominal DCE-MRI datasets which employs signal intensity corrections and a floating reference image scheme. We perform a preliminary quantitative validation of this registration technique using an abdominal DCE-MRI dataset with a known amount of simulated motion.

2. METHODS

Image registration was framed in terms of an optimization problem. Consider the task of registering some moved image volume T to a reference image volume R. A deformation (y) must be found that minimizes

$$J(y) = D(T(y), R) + \alpha S(y). \quad (1)$$

$T(y)$ represents the image volume T which has been deformed by y. D is a distance measure which quantifies the similarity between $T(y)$ and R. $S(y)$ is a regularizing term which quantifies the suitability of the deformation y. High values of D and S correspond to dissimilar image volumes and unsuitable transformations respectively. Finally, α is a weighting parameter for the regularizing term. D was chosen to be the computationally fast sum of squared differences (SSD). Traditionally it is the high sensitivity of the SSD to intensity changes which makes it a poor distance measure within the contrast-enhanced registration setting. However, in the presence of an intensity correction term, such sensitivity may be desirable. $S(y)$ was chosen to be the commonly used elastic regularizer [2,5].

The Flexible Algorithms for Image Registration (FAIR) toolkit was built upon this framework and was therefore used in this study to perform deformable registration [5].

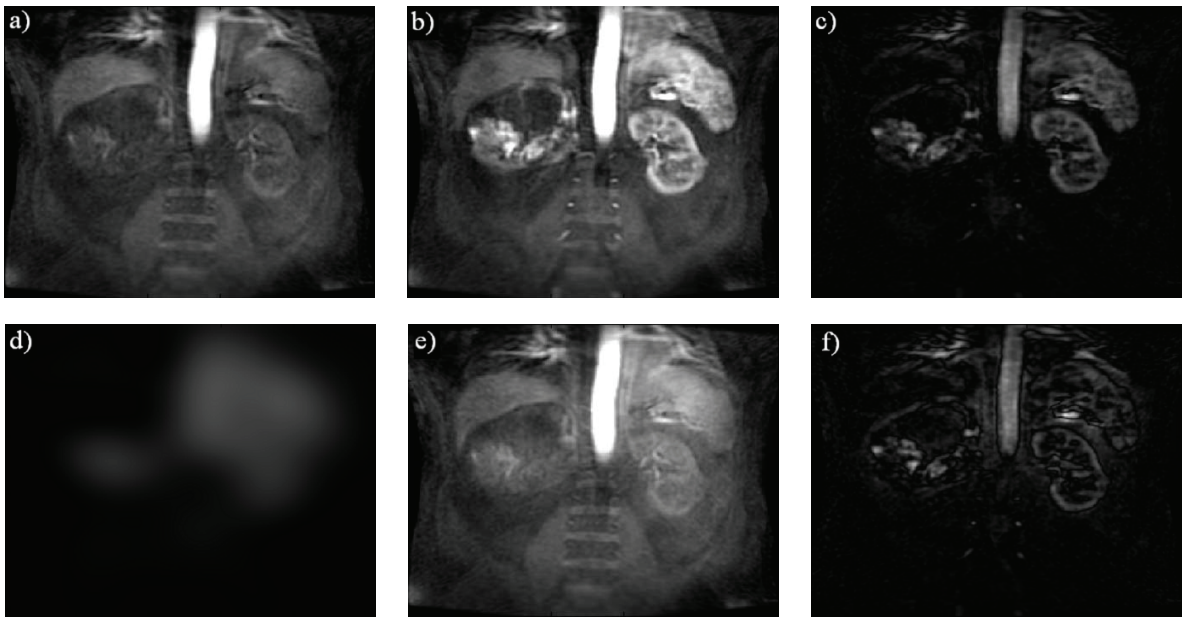

Figure 1 2D intensity correction example from an abdominal DCE-MRI dataset. a) T b) R c) $|R-T|$ d) c e) T^c f) $|R-T^c|$

FAIR contains a suite of interchangeable MATLAB functions that can be used for various image registration tasks. The presented algorithm modifies input image data and adapts the functionality of the FAIR toolkit to better suit the contrast enhanced-image registration setting.

Elastic regularizer parameters were set to the FAIR default of [μ, λ] = [1, 0] with the dataset intensities being scaled between 0 and 255. The parameter α was chosen experimentally through trial and error and was set to 100, 600, and 200 for registration of pre-enhancement, wash-in, and wash-out volumes respectively. Multilevel optimization was employed in order to smooth the optimization problem and increase speed [5]. An initial rigid registration is performed prior to this optimization in order to correct for large-scale motion. The optimizer was chosen to be the limited memory Broyden-Fletcher-Goldfarb-Shanno method (l-BFGS) which is well suited to working with large image datasets [6].

2.1. Intensity Correction

A simple intensity correction has been developed in order to partially account for the intensity differences between image volumes within the contrast-enhanced setting. Instead of finding the deformation that optimally matches T and R in terms of (1), we search for the deformation that optimally matches T^c and R where

$$T^c = T + c \tag{2}$$

$$c = (R - T) * N(0, \sigma) \tag{3}$$

and $N(0,\sigma)$ is a Gaussian blurring kernel with zero mean and standard deviation σ. The resulting optimal deformation is then applied to the original image volume T.

The standard deviation σ was defined such that full-width half max was half of the kernel size. The kernel size was chosen to be 150.4mm by 150.4mm by 40mm in the superior-inferior (S/I), left-right (L/R), and anterior-posterior (A/P) directions respectively. This size was chosen to be large enough to ensure that the correction term did not contain high-contrast edge information. Such information can be spatially inaccurate up to the magnitude of the motion present between the two image volumes. Furthermore the intensities may not reflect the actual enhancement since structures do not overlap perfectly in the initial subtraction volume. Consequently this information is significantly blurred in order to reflect its high uncertainty.

The correction term reduces the contribution of intensity differences caused by the contrast agent to the SSD distance measure. Consequently unenhanced regions of the image volume play a greater relative role in informing the image registration. This is desirable since intensity changes in these regions are solely due to patient motion which presents a much simpler registration task. An example is illustrated in figure 1 using a coronal slice from a 3D abdominal T1-weighted DCE-MRI dataset acquired with a fast spoiled gradient-echo sequence (FSPGR). Figures 1c and 1f show how the relative enhancement between the two images is reduced after intensity correction.

The intensity correction should not need to be applied when registering volumes acquired prior to the injection of the contrast agent. However, there are significant intensity changes in wash-in and to a lesser extent in the wash-out enhancement phases where the intensity correction is needed.

2.2. Registration Scheme

In an effort to further minimize the intensity differences due to contrast enhancement between T^c and R, we employ a floating reference image registration scheme (figure 2). Consider a DCE-MRI dataset $V = \{ v_i \}$, $i = 1 \ldots n$, where v_i corresponds to the i-th MRI volume acquired in time. Let v_p be a single volume selected from V. First, the two volumes adjacent in time to v_p (v_{p-1}, v_{p+1}) are registered to v_p, producing $(v_{p-1})_{reg}$ and $(v_{p+1})_{reg}$. Next, v_{p-2} and v_{p+2} are registered to $(v_{p-1})_{reg}$ and $(v_{p+1})_{reg}$ respectively producing $(v_{p-2})_{reg}$ and $(v_{p+2})_{reg}$. This process continues until all the volumes have been registered.

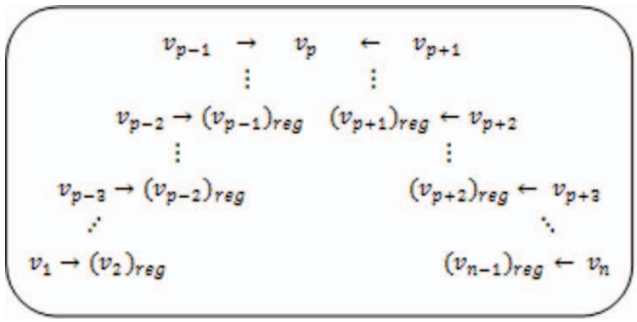

Figure 2 Floating reference image registration scheme. Arrows denote registration. Subscript '*reg*' denotes registered version of the volume.

Here the reference image volume for every registration is different. Assuming accurate registrations, all v_i should be registered to v_p since this scheme proceeds serially.

We chose v_p to correspond to the image volume with the highest average voxel intensity. As the contrast agent flows into the patient, anatomical structure becomes more apparent in the image volumes. Therefore v_p is liable to contain the most detail and may serve as a suitable starting point for this scheme.

2.3 Preliminary Validation

Our preliminary validation approach involves both subjective and quantitative components. The proposed image registration algorithm is first applied to real clinical datasets. The results are visually evaluated to ensure that the algorithm can account for real patient motion and complex enhancement patterns. For quantitative validation, a known amount of simulated motion is added to a motionless clinical dataset. Image registration is subsequently applied and the recovered transformation is compared with the known simulated motion field.

The motionless dataset needs to be constructed since in principle, there is always some motion present in DCE-MRI datasets. To construct the motionless dataset, two approaches were combined. First, the aforementioned image registration technique was applied to the dataset to remove the bulk of the naturally occurring motion. Second, principal components analysis (PCA) reconstruction was applied to the registered dataset to further eliminate motion.

In short, a dataset can be expressed as a linear combination of the eigenvectors of its covariance matrix. The principal components are the terms in this linear combination which correspond to the eigenvectors with the largest associated eigenvalues. These principal components contain the primary sources of variance within the dataset. If it is assumed that changes in the dataset due to motion are uncorrelated then reconstructing the data using a linear combination of only the principal components can eliminate motion [3, 4]. Motion in abdominal datasets is largely due to respiration and is therefore at least partially correlated in time. Consequently this technique may not be able to remove highly correlated respiratory related motion. The registration performed prior to PCA reconstruction helps to mitigate this potential problem by reducing the magnitude of correlated motion. Simulated motion was introduced to the motionless dataset using a coarse approximation to the non-rigid S/I motion introduced by the diaphragm combined with rigid rotations about the S/I axis. The S/I displacements were modelled by

$$\Delta \mathrm{SI}(\mathrm{x}, \mathrm{t}) = \Delta \mathrm{SI}_{\max} \sin\left(\frac{\pi x}{x_{max}}\right) \left|\sin\left(\frac{\pi \mathrm{t}}{\mathrm{t_b}}\right)\right| \qquad (4)$$

where x corresponds to L/R position, t corresponds to time, $\Delta \mathrm{SI}_{\max}$ is the maximum S/I displacement, x_{max} is the maximum L/R extent of the patient, and $\mathrm{t_b}$ is the time taken per full breath (inhale and exhale). The angle of the rigid rotation was modelled by

$$\theta(\mathrm{t}) = \left|\sin\left(\frac{\pi \mathrm{t}}{\mathrm{t_b}}\right)\right| \theta_{\max} \qquad (5)$$

where the maximum rotation angle is given by $\theta_{\max}$. Rotations are larger if a deeper simulated breath is taken. The parameters $\Delta \mathrm{SI}_{\max}$ and $\theta_{\max}$ were chosen to be 15mm and 1.5° respectively.

To better simulate natural respiration, the respiration rate ($1/\ \mathrm{t_b}$) was sampled from a normal distribution with $\mu = 15$ breaths/second [1] and $\sigma = 2$ breaths/second. A new respiration rate was sampled after every simulated breath.

2.4. Patient Data

10 clinical DCE-MRI scans of the abdomen were used to develop and test the proposed image registration algorithm. The scans were acquired with a T1-weighted FSPGR sequence. Spatial resolution was 1.88mm by 1.88mm by 8mm in the S/I, L/R, and A/P directions respectively. Temporal resolution was approximately 3.7 seconds per volume.

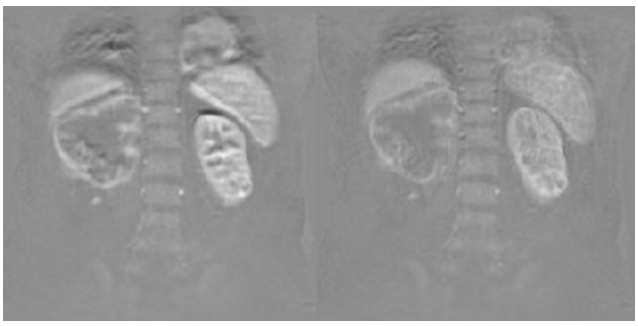

Figure 3 Example of a subtraction image before and after registration.

3. RESULTS

Registration effectively eliminated visual motion within all 10 clinical datasets. Inspection of subtraction images revealed significant reduction in motion artifacts (figure 3). A 5 voxel region of interest (ROI) was selected within a highly enhancing renal tumour present within one of the datasets in order to investigate registration effects on intensity-time curves. The ROI average intensity-time curve acquired from subtraction image volumes was plotted before and after registration (figure 4). Prior to registration, the actual ROI moves in and out of the investigated region obscuring trends. After registration, a more typical intensity-time curve emerged.

Preliminary validation was performed using one of the previously registered clinical datasets. The registered dataset was reconstructed using the first four principal components. Remaining visual motion was limited to the flow of the contrast agent through the patient, which maintained similar complexity to the flow within the actual DCE-MRI dataset.

Simulated motion was introduced to the motionless dataset. The distances of the voxels from their initial location in the motionless dataset were calculated before and after registration (table 1).

Table 1 Average distance of voxels from their initial location, before and after registration. Standard deviations are shown in brackets.

Type	Distance (mm)	
	Before	After
S/I	6.1(4.6)	2.1(2.1)
A/P	2.0(1.7)	1.8(1.4)
L/R	0.4(0.3)	1.1(1.9)
Total	6.7(4.6)	3.4(2.7)

After image registration, the average distance and standard deviation decreased in the S/I and A/P coordinate directions, but increased in the L/R direction. Approximately half of the total voxel distance (motion), was corrected for by image registration. Despite this remaining discrepancy, no easily identifiable visual motion was present within the registered result.

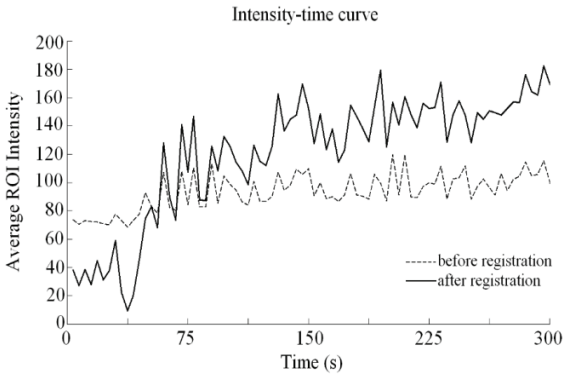

Figure 4 Effect of registration on the intensity-time curve of a 5 voxel ROI.

The total distance was then further broken down by volume to investigate how different motion magnitudes were addressed by the image registration (figure 5). The algorithm was able to correct for different magnitudes of motion, but had a more pronounced effect on voxels which had been displaced by higher magnitudes.

4. DISCUSSION

The algorithm was applied to clinical datasets with and without the use of intensity correction. Without intensity correction, registration failed to eliminate motion as was evident by little apparent reduction in visual motion as well as output deformations which led to limited voxel displacements. Registration performed marginally better in the wash-out phase since intensity changes are more gradual than in the wash-in phase. With intensity correction, registration performed well in removing visual motion in the clinical datasets and the validation test case. Despite this, the average remaining motion within the test case was found to be on the order of 3.4mm (σ = 2.7mm). This remaining discrepancy could be attributed to poor regularizer performance. Within a near uniform intensity structure, voxels do not necessarily have to be mapped to their original location for the SSD distance measure to be reduced. In this case, the burden of ensuring proper voxel mapping falls upon the regularizer. Therefore if the regularizer fails, the registered dataset could appear well-registered despite the validation showing otherwise.

Furthermore, the multi-level image registration was allowed to proceed until a 128 by 128 by 32 discretization level was reached. This corresponded to a consideration of 3.76mm by 3.76mm by 3mm voxels. Therefore it is not surprising that the registration was unable to correct motion to much below the dimensions of the voxels. This may also explain the increase in voxel distance in the L/R coordinate direction since the uncorrected distance was well below the size of the voxel dimensions. Increases in registration accuracy are predicted upon permitting a higher final level

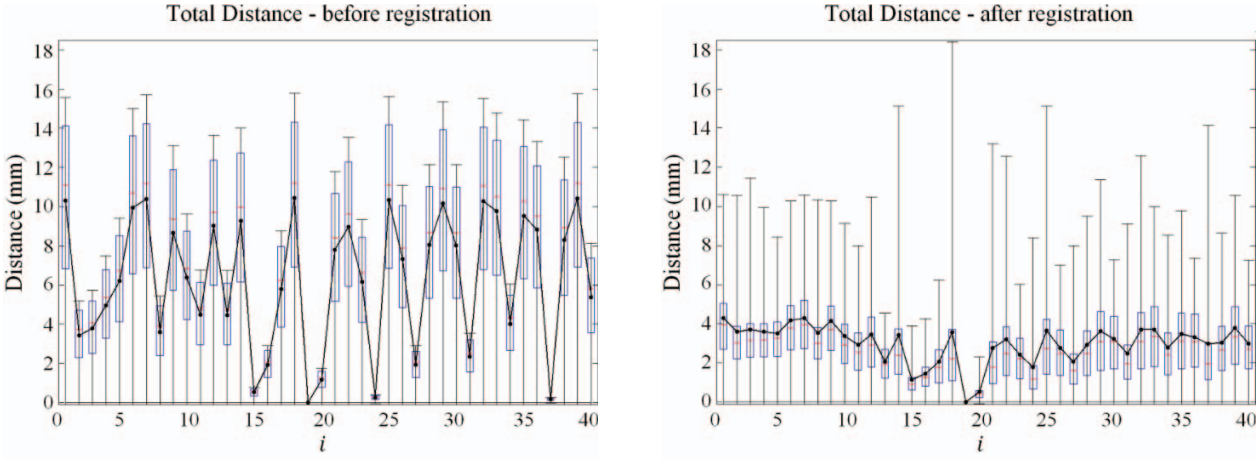

Figure 5 Distribution of the distance of the voxels in v_i from their initial location in the motionless dataset, before and after registration. Box plots indicate the first three quartiles. Whiskers encompass 95% of all values. The average value is displayed with a thick black line. $v_p = v_{19}$.

of optimization. A higher level was not investigated within this study because the FAIR toolkit has not yet been optimized for computation speed. Addressing higher discretization levels became increasingly computationally prohibitive.

Despite this, the proposed registration algorithm is simple and computationally inexpensive as it only involves a preparation of the data prior to registration and does not alter the underlying optimization framework in any way. Consequently, it should be easily adaptable to other image registration frameworks. Furthermore there are opportunities for parallelizing this algorithm. Image volumes could be registered in parallel, and then the resulting deformations could be combined afterwards to register each volume to the reference volume. This could increase the computation speed by a factor equal to the number of computer threads. Future work will be undertaken to incorporate the intensity-correction term into the optimization procedure such that it is re-estimated after each iteration.

The procedure to create the motionless dataset for validation was very effective at removing visual motion. It must still be determined whether this algorithm is appropriate for use in registering real patient datasets for the purposes of DCE-MRI analysis. Quantitative validation may be difficult within this context as a gold standard is not available.

5. CONCLUSIONS

We have presented a simple, computationally inexpensive, algorithm for registering abdominal DCE-MRI datasets. Visual motion was significantly reduced within the investigated datasets, and a positive effect on the intensity-time curve of a small ROI was observed. The algorithm addressed approximately half of the total motion simulated within the preliminary quantitative validation and no easily identifiable visual motion was present after registration. The technique should be easily applied within other image registration frameworks. Further validation using datasets from different anatomic sites is necessary and will be undertaken in the future. Improved motion models based on finite element modeling will be used to further verify utility.

6. ACKNOWLEDGEMENTS

This work was supported by the Terry Fox Foundation.

7. REFERENCES

[1] B. Beckett, *Illustrated Human and Social Biology*, Oxford University Press, Oxford, April 1999

[2] C. Broit, "Optimal registration of deformed images", Ph.D thesis, University of Pennsylvania, Philadelphia, 1981

[3] A.L. Martel, M.S. Froh, K.K. Brock, D.B. Plewes, D.C. Barber, "Evaluating an optical-flow based registration algorithm for contrast-enhanced magnetic resonance imaging of the breast. *Phys. Med. Biol.*, IOP Publishing LTD, England, May. 2007

[4] A. Melbourne, D. Atkinson, M. J. White, D. Collins, M. Leach, D. Hawkes, "Registration of dynamic contrast-enhanced MRI using a progressive principal component registration (PPCR)", *Phys. Med. Biol.*, IOP Publishing LTD, England, Sep. 2007

[5] J. Modersitzki, *FAIR: Flexible Algorithms for Image Registration,* SIAM, Philadelphia, 2009

[6] J. Nocedal, S.J. Wright, *Numerical optimization*, Springer, New York, 1999

[7] J.P.B O'Connor, A. Jackson, G.J.M. Parker, G.C. Jayson, "DCE-MRI biomarkers in the clinical evaluation of antiangiogenic and vascular disrupting agents," *Brit. J. Cancer*, Nature Publishing Group, London, pp. 189-195, Jan. 2007